Pedotransfer Functions for Permeability: A Computational Study at Pore Scales

Jeffrey D. Hyman[1], Piotr K. Smolarkiewicz[2], C. Larrabee Winter[1,3]

Jeffrey D. Hyman, Program in Applied Mathematics, University of Arizona, Mathematics Building, Tucson, AZ, 85721, USA. (jhyman@math.arizona.edu)

Piotr K. Smolarkiewicz, Mesoscale and Microscale Meteorology Division, National Center for Atmospheric Research, Boulder, CO, 80307, USA. (smolar@ucar.edu)

C. Larrabee Winter, Department of Hydrology and Water Resources, Program in Applied Mathematics, University of Arizona, Harshbarger Building 11, Tucson, AZ, 85721, USA. (winter@email.arizona.edu)

[1]University of Arizona, Program in Applied Mathematics, Tucson, AZ, 85721, USA.

[2]National Center for Atmospheric Research, Boulder, CO, 80307, USA.

[3]Department of Hydrology and Water Resources,University of Arizona, Tucson, AZ, 85721, USA.

Abstract. Three phenomenological power law models for the permeability of porous media are derived from computational experiments with flow through explicit pore spaces. The pore spaces are represented by three dimensional pore networks in sixty-three virtual porous media along with fifteen physical pore networks. The power laws relate permeability to (i) porosity, (ii) squared mean hydraulic radius of pores, and (iii) their product. Their performance is compared to estimates derived via the Kozeny equation, which also uses the product of porosity with squared mean hydraulic pore radius to estimate permeability. The power laws provide tighter estimates than the Kozeny equation even after adjusting for the extra parameter they each require. The best fit is with the power law based on the Kozeny predictor, that is, the product of porosity with the square of mean hydraulic pore radius.

1. Introduction

Flows of fluid through a porous medium are distinguished from flows through open bodies by spatially variable resistance arising from variations in the medium's pore space geometry and topology that yields a steady flow. At pore-resolving scales a porous medium is a network of explicit, interconnected channels embedded in a solid medium. Critical parameters affecting resistance in pore spaces include typical radius of the pores, the length of a streamline between two points relative to the distance between the points, and the density of pores. Sample volumes ranging from 0.01-1000 cm^3 are typical of laboratory pore space experiments with most at the lower end of the range. At macroscopic scales, porous media are usually represented as volumes with system states, e.g. velocity and hydraulic head, and parameters, e.g. permeability and porosity, defined piece-wise continuously at every point in the volume. Macroscopic resistance to flow is quantified by its approximate inverse, permeability, which is defined via Darcy's law in terms of the ratio of fluid flux to the gradient of pressure within the fluid. Darcy's law was established experimentally [*Darcy*, 1856] and later derived analytically by upscaling pore-network flows through homogenization, or volume averaging [*Shvidler*, 1964; *Whitaker*, 1999]. Alternatives based on ensemble averaging have also been used to estimate permeability from pore-scale properties of porous media [*Rubinstein*, 1986].

Although permeability is a well-established property of most relatively uniform porous media, its actual dependence on specific geometric and topological properties of porous networks is not fully understood. Phenomenological transfer functions have been developed by soil physicists, hydrologists, chemical and petroleum engineers, and materials scientists to estimate permeability from properties of porous media that are relatively easy to observe. A natural starting point is to suppose that a sample volume's permeability is proportional to its porosity since the latter indicates pore density and is a good measure of the medium's capacity to hold fluid. Yet this is not entirely satisfactory, since two porous media can have the same porosity but one may be entirely impermeable while the other offers minimal resistance to flow.

Perhaps the best known phenomenological transfer functions are the Kozeny equation [*Kozeny*, 1932; *Carman*, 1956; *Bear*, 1988] and the Kozeny-Carman equation [*Carman*, 1939]. Kozeny derived his equation,

$$k = c_0 n R^2, \tag{1}$$

by reasoning about flow through an idealized pore network: he equated the velocity given by Poiseuille's law for flow through a bundle of capillary tubes to the specific discharge obtained from Darcy's law and thus solved for permeability. He concluded that permeability, k, is proportional to the product of porosity, n, with the square of mean hydraulic radius, R, a measure of typical pore size. Hence, the Kozeny predictor, nR^2, combines a factor, n, depending on the capacity of a medium to hold fluid with another, R, depending on the ability of the medium to transmit it. The dimensionless constant, c_0, is known as the Kozeny coefficient. *Carman* [1939] extended (1) by including a factor of tortuosity, τ, an index of the complexity of streamlines in the medium, and derived the Kozeny-Carman equation

$$k = c_0' n R^2 / \tau^2. \tag{2}$$

Since permeability is a characteristic of a porous medium, (1) and (2) need to be properly scaled by fluid viscosity and density to relate a medium's permeability to its saturated hydraulic conductivity with respect to a particular fluid.

We follow *Smolarkiewicz and Winter* [2010], [*SW10*] for brevity, and determine permeability computationally by simulating the basic elements of Darcy's original experiment [*Darcy*, 1856] in three-dimensional networks of pores, allowing pore-scale processes to be observed in detail. *Hyman et al.* [2012], hereafter [*HSW12*], employed the techniques of [*SW10*] to study the influence of porosity on the degree of heterogeneity in steady state flows within stochastically generated three dimensional pore networks. [*HSW12*] reports technical aspects of modeling flow in explicit pore spaces and provides a Lagrangian perspective of the pore space via particle tracking. That paper focuses on heterogeneity of microscopic flow field and its relationship to porosity, while this paper focuses on the continuum scale properties of permeability. They quantify the degree of heterogeneity in the flow and identify coherent heterogeneities in the flow field by tracking fluid particles and recording various attributes including tortuosity, trajectory length, and first passage time in media with porosities between 0.2 and 0.7.

Here, the techniques of [*SW10*] are used to estimate overall permeability for each of seventy-eight small, $O(1\mathrm{cm}^3)$, sample volumes of porous media. Sixty-three realizations are drawn from ensembles of virtual pore spaces with porosities ranging from 0.19 to 0.84, while the others are a volcanic tuff [*Wildenschild et al.*, 2004], a column of glass beads [*Culligan et al.*, 2004], and thirteen unique sandpacks, sandstones, and carbonate from *Mostaghimi et al.* [2013]. Virtual pore spaces are isotropic and statistically stationary in space with permeabilities corresponding to a well-sorted gravel or sand [*SW10*];

[*HSW12*] demonstrated that the virtual media are large enough to constitute representative elementary volumes. Their material properties appear consistent with those of the glass beads and tuff. Owing to the high resolution of the seventy-eight pore space samples, porosity and hydraulic radius can be directly evaluated.

The computed permeability, porosity, and hydraulic radii of the virtual media are used to empirically estimate the Kozeny coefficient, c_0. The estimate $\hat{c}_0 = 0.19$ is in excellent agreement with Carman's original value, $c_0 = 0.2$, indicating the representativeness of the virtual pore spaces. Additionally, over a restricted range of porosities, $0.2 < n < 0.7$, the analytically derived Kozeny and Kozeny-Carman laws are both reproduced reasonably well. The Kozeny equation (1) fits results from media with porosities in $0.2 < n < 0.7$ fairly well and the Kozeny coefficient is within an interval later noted by noted by *Carman* [1956]. The Kozeny-Carman equation (2) also predicts permeability adequately within this limited range and the computed coefficient, c'_0, is near that suggested by Carman.

Yet the Kozeny equation is not entirely satisfactory as a predictor of permeability for the entire data set. Plotting the permeability data against the Kozeny predictor, nR^2, reveals an obvious nonlinearity at large and small values of nR^2 that is not captured by the linear (in the predictor) Kozeny model. Hence, scale-invariant power law alternatives depending upon porosity, n, the square of hydraulic radius, R, and the Kozeny predictor, nR^2, that is their product, are derived and compared to the Kozeny equation. Focus is placed on the Kozeny equation and related power laws rather than the Kozeny-Carman equation because the tortuosity of the data is highly correlated with porosity and mean hydraulic radius.

The power law alternatives provide better fits to the physical and virtual data, although at the expense of adding an extra parameter, than does the Kozeny equation over the entire range of data. We attribute this to the ability of simple power laws to capture the nonlinear effects of pore space interconnectivity on permeability at extremes of porosity and mean hydraulic radius. This seems born out by a power law based on the Kozeny predictor, nR^2, which yields a sum of squared errors for the virtual data that is significantly smaller than the errors of power laws based on porosity or mean hydraulic radius alone. Goodness of fit and model performance for these data are evaluated using a standard statistical technique, the Analysis of Variance, to gauge the relative advantage conferred by the additional parameter. The overall fit of the models to both real and synthetic data is evaluated and compared using chi-squared tests.

Section 2 reviews previous studies to determine permeability computationally and places the present work within context of the previous studies. Section 3 describes simulations of pore networks and flow; computational methods for generating virtual porous media along with a characterization of the physical data (Section 3.1), numerical techniques for resolving flow in the explicit pore networks (Section 3.2), and estimation of transfer function variables including porosity, hydraulic radius, tortuosity, and permeability (Section 3.3-3.4). A preliminary study to determine a proper grid resolution for the study is performed prior to derivations of the power law alternatives to the Kozeny equation (Section 3.5). Next the empirical pedotransfer functions are derived and evaluated (Section 4.1), and their ranges of applicability are discussed (Section 4.2). We finish with a summary of the experiment and offer a few remarks about the generality of the results in Section 5.

2. Background

Pedotransfer functions are mathematical or computational models used to estimate hydraulic soil properties, e.g. saturated hydraulic conductivity, on the basis of pedological data [*Wösten et al.*, 2001; *Schaap et al.*, 2001], and are commonly derived empirically using soil samples in continuum scale laboratory experiments where k, n, R, and τ are measured in bulk. Computational experiments with flow at the pore-scale allow these quantities to be observed in detail and generalized pedotransfer functions to be empirically derived at scales similar to those Kozeny and Carman considered but in more complicated networks.

The Kozeny (1) and and Kozeny-Carman (2) equations are generalized pedotransfer functions for predicting permeability, a macroscopic soil property, derived analytically via considerations of microscopic pore scale dynamics (they are general in the sense that the predictors are not specific to a particular type of soil); *Lebron et al.* [1999] and *Rawls et al.* [2005] provide comparisons between (1), (2) and other pedotransfer functions.

2.1. Permeability Based on Pore-scale Simulations

Computational solutions for the flow of a viscous fluid through an explicit pore space go back at least to *Hasimoto* [1959] who solved for flow in a periodic array (cubic) of spheres by deriving the fundamental solution to the Stokes equations using Fourier transforms. He also obtained an expression for drag by expanding the velocity profile in terms of the fundamental solution and its derivatives. *Launder and Massey* [1978] numerically solved the Navier-Stokes equations for flow through a periodic array of long cylinders with known geometric configurations. *Sangani and Acrivos* [1982a, b] and *Zick and Homsy* [1982] computed Stokes drag on slow flows in porous media composed of simple elements like spheres. Permeability has been estimated by simulating flow through more realistic pore networks by *Lemaitre and Adler* [1990], *Fourie et al.* [2007], [*SW10*], and *Mostaghimi et al.* [2013] to name a few. *Fourie et al.* [2007] found good agreement between their numerical estimates and measured permeabilities for a small volume of coarse sand (0.81 mm on a side). *Matyka et al.* [2008] and [*HSW12*] found evidence for the existence of representative elementary volumes in simulated flows through realistic random pore networks. *Meakin and Tartakovsky* [2009] provide a current discussion of other methods for modeling flow in porous networks.

The behavior of the Kozeny equation has been investigated through computational experiments with flow in random or fractal pore networks. Scaling arguments indicate good agreement between the Kozeny coefficient, c_0, and data obtained from computational experiments with flow through networks based on Sierpinski carpets [*Adler and Jacquin*, 1987]. On the other hand, *Adler et al.* [1990] found that the Kozeny coefficient is about half the standard value of 1/5 given by *Carman* [1939] when based on simulations of flow through random media with statistics like Fontainbleau sandstone. *Lemaitre and Adler* [1990] discovered that agreement between observed and theoretical values of the Kozeny coefficient varied according to the porosity of networks they simulated: the Kozeny equation did not hold for random media at relatively high or low porosities (in the latter case, close to the percolation threshold they used to generate random media), nor did it hold for media generated from regular fractals when the largest pores were held constant as resolution was increased. The simulations performed in this paper also indicate nonlinear behavior of permeability at high and low porosities, and also at extremes of mean hydraulic radii.

2.2. Physical Evidence for Kozeny Equation

The Kozeny and Kozeny-Carman equations have been validated and verified in experiments with flow through physical media composed of arrays of glass beads, other shapes like rods, and natural porous media [*Carman*, 1956; *Bear*, 1988]. Soil scientists have shown that (1) and (2) provide estimates of permeability that are superior to some other soil transfer functions [*Chapuis and Aubertin*, 2003; *Dvorkin*, 2009]. The estimate given by *Carman* [1939] of $c_0 = 1/5$ for the Kozeny coefficient seems adequate for media in a middle range of porosity ($0.2 < n < 0.7$) [*Xu and Yu*, 2008]. In some circumstances high correlation between tortuousity and porosity makes the simpler Kozeny equation a cost-effective alternative to the Kozeny-Carman equation [*Koponen et al.*, 1996].

The Kozeny and Kozeny-Carman equations have been found, however, to yield poor estimates of permeability at the extremes of porous medium types: either when total fluid discharge through a porous medium is negligible or at the other extreme where the effect of the medium on the overall flow is local and small [*Kyan et al.*, 1970; *Xu and Yu*, 2008]. These results are consistent with the pore-scale computational experiments of *Lemaitre and Adler* [1990] mentioned above and the experiments reported here. *Heijs and Lowe* [1995] found that the Kozeny-Carman equation predicted the permeability of a particular random array of spheres well (porosity $n = 0.6$), but failed to do so in a soil sample that had porosity near one. *Sullivan* [1942], *Kyan et al.* [1970], *Davies and Dollimore* [1980] and *Xu and Yu* [2008] all note that the Kozeny coefficient varies nonlinearly with porosity and most significantly at its extreme values.

2.3. Alternatives to Kozeny Equation

Efforts have been made to compensate for these weaknesses by modifying the Kozeny and Kozeny-Carman equations. The Kozeny-Carman equation has been expanded to include effective porosity [*Koponen et al.*, 1997], percolation threshold and geometric properties of the pore network [*Nabovati et al.*, 2009], and fractal geometry [*Xu and Yu*, 2008]. However *Schaap and Lebron* [2001] found that modifications do not always improve on estimates given by (1) and (2). *Revil and Cathles* [1999] derive a power-law relation,

$$k \propto d^2 n^{3m}, \tag{3}$$

between permeability of a clay-free sand, k, and grain diameter, d, and porosity, n, based on an electrical cementation exponent, m, that reflects the connectivity of the pore space. Their method depends on the Archie relationship [*Archie*, 1942],

$$n = \mathcal{F}^m, \tag{4}$$

that expresses porosity as a power of an electrical formation factor, $\mathcal{F}$, whose reciprocal quantifies the effective interconnected porosity of a porous medium. Values of m vary between 1 and 4 according to *Sen et al.* [1981]. *Revil and Cathles* [1999] derive power laws for permeability of a pure shale and sand-shale mixtures in a similar way with the specific value of m depending on the porous material. Jacquin [1964] quoted in [*Adler et al.*, 1990] found evidence for

$$k \propto n^{4.15} \tag{5}$$

for samples of Fontainbleau sandstone. *Lemaitre and Adler* [1990] indicate that permeability behaves like a power of porosity near the percolation limit (the value of porosity below which there are no continuous pore channels through one of their realizations) of the random porous media they construct. Other variants of the Kozeny equation that depend solely on porosity have been proposed by *Nielsen et al.* [1984] and *Ahuja et al.* [1989].

In sum, estimates of permeability based on the Kozeny and Kozeny-Carman equations are reasonably accurate when applied to an intermediate range of porosities. This is true for simulations based on pore-scale flows and physical experiments at laboratory scales. For low porosity porous media like the Fontainbleau sandstone, shales, or sand-shale mixtures, however, estimates of permeability based on the Kozeny equation are frequently inaccurate, probably because linear dependence on porosity and the square of mean hydraulic radius (R^2) does not completely capture the detailed effects of interconnectivity within a pore network. When interconnectivity is accounted for by means of a formation factor, permeability is fairly well captured by a power law based on porosity. The effect that (squared) mean hydraulic radius has on permeability is not as well-established in the literature as the effect of porosity. *Revil and Cathles* [1999] include it as a linear factor in the porosity-based power law that they propose.

3. Simulation of Pore Network Flow and Permeability

First we provide the methods used to generate the virtual porous media and describe the physical data samples. Next, the procedure used to numerically integrate the Navier-Stokes equations within the explicit pore spaces is sketched, (see [*SW10*] for a complete description). Last, we detail the methods for observing and estimating variables of the pedotransfer functions.

3.1. Porous Media

The seventy-eight three dimensional porous media used as data sets for this study are comprised of a volcanic tuff, a column of glass beads, thirteen unique sandpacks, sandstones, and carbonates provided in Table 2 of *Mostaghimi et al.* [2013], and sixty-three realizations drawn from ensembles of virtual porous media with specified expected geometry and topology.

3.1.1. Virtual Porous Media

Each virtual porous medium is a three-dimensional pore space with sides of length $L_x = L_y = 1.27$ cm, height $L_z = 2.55$ cm, and volume $V = 4.11\text{cm}^3$ with individual pore areas typically 1-10 μm^2 at a horizontal cross section. Level-set percolation [*Alexander and Molchanov*, 1994; *Alexander*, 1995] is used to generate realizations of porous media from underlying random topographies.

To generate each virtual pore space realization, independent identically distributed random values are sampled uniformly on the interval $[0, 1]$ and one value, $f_{\mathbf{i}}$, is assigned to each node, $\mathbf{i}$, on a three-dimensional grid. Correlated random topographies are generated from $f_{\mathbf{i}}$ using three different methods. In the first method, $f_{\mathbf{i}}$ is convolved with a symmetric Gaussian kernel to generate an isotropic correlated random topography by transforming $f_{\mathbf{i}}$ into frequency space, multiplying it by a Gaussian function, and then transforming it back into real space. The correlation length of this random topography is determined by the standard deviation of the Gaussian function which is fixed at $\sigma = 0.01$; see [*HSW12*] for details of this method. In the second method, a uniform kernel is applied by uniformly weighting every point in a cube centered on $\mathbf{x}$ with sides of length $l = 4$. In the third method the random field $f_{\mathbf{i}}$ is low-pass filtered using m consecutive applications of the tensor product $f^{flt} = f^{fltx} \otimes f^{flty} \otimes f^{fltz}$; see [*SW10*] for details of this method. Here, the symmetric weighting operator sweeps over $f_{\mathbf{i}}$ four times, $m = 4$. Values of $\sigma = 0.01$, $l = 4$, and $m = 4$ are chosen so the correlation lengths of realizations are approximately the same, ~ 0.05 cm. Since the convolution kernels have unit $\mathcal{L}^2$ norm the convolutions do not change the expected value or range of the topographies. Moreover, the central limit theorem implies that all three methods yield topographies whose elements are approximately Gaussian.

A pore space realization is derived by applying a level threshold, $\gamma \in [0, 1]$, to each node value in the topography. If the value at the node is greater than γ, then the node is placed in the solid matrix, otherwise it is in the void space. For physical intuition, γ can be thought of as a control parameter which determines the expected porosity of a pore space realization (Fig. 1), the exact linear relationship between the two is given in Section II. A of [*HSW12*]. As γ increases, porosity and hydraulic radius also increase, while tortuosity decreases (Table 1). The result of applying this level set percolation method is a statistically stationary pore volume in the sense that the finite-dimensional probability distributions of pore space membership are invariant with respect to translation in space.

The level threshold determines the flow volume, the geometric properties of porosity and mean hydraulic radius, and topological properties such as the number of connected pore channels and number of connected solid components. Another topological effect of the level threshold is revealed by the existence of a percolation limit for topographies generated by a given kernel, a threshold below which no amount of pressure will drive significant flows through a pore space realization. At high values of the threshold parameter the flow regime resembles slow flow around disconnected bodies with Reynolds numbers ranging between 1 and 2.

3.1.2. Physical Porous Media

The tuff data comes from a 0.34cm^3 sample volume with porosity 0.37 [*Wildenschild et al.*, 2004], and the glass beads are from a sample volume of 0.032cm^3 with porosity 0.31 [*Culligan et al.*, 2004]. Horizontal cross sections of these physical media are shown in Fig. 2. *Mostaghimi et al.* [2013] obtain binarized three dimensional rock images of six sandpacks, five sandstones, and two carbonantes using micro CT imaging, and determine the permeability of the thirteen samples by numerically solving the Stokes equations in the void space to attain steady state flow and pressure fields and then inverting Darcy's law. The samples' porosity, specific surface, and permeability are provided in Table 2 of *Mostaghimi et al.* [2013].

3.2. Computational Fluid Dynamics

Flow in the virtual media is simulated by numerically solving the incompressible Navier-Stokes equations on a Cartesian domain with dimensions $L_x = L_y = 1.27$ cm and $L_z = 2.55$ cm, and volume $V = 4.11\text{cm}^3$. The grids have 128 nodes in the horizontal directions and 256 in the vertical direction. Computational limitations require that sub-volumes of the beads and tuff be extracted from the center of the entire sample. Each medium, whether virtual or physical, is periodic in the vertical direction with no flow allowed across lateral boundaries. The real media are reflected across a horizontal plane to create periodic boundaries in the vertical; *Siena et al.* [2012] demonstrated that this reflection does not affect results.

The multi-scale computational fluid dynamics modeling system EULAG [*Prusa et al.*, 2008] is used to solve the governing Navier-Stokes equations for water flow, as in [*SW10*] and [*HSW12*], and the three components of velocity and pressure gradient are computed at every point within each porous medium. The EULAG system accommodates a broad class of flows and underlying fluid equations in a variety of domains on scales ranging from wind tunnel and laboratory [*Wedi and Smolarkiewicz*, 2006; *Smolarkiewicz et al.*, 2007; *Waite and Smolarkiewicz*, 2008] through terrestrial environments and climate [*Grabowski and Smolarkiewicz*, 2002; *Abiodun et al.*, 2008a, b; *Ortiz and Smolarkiewicz*, 2009], to stellar [*Ghizaru et al.*, 2010].

3.2.1. Immersed Boundary Method

The crux of our computational approach for simulating flows in porous media is an immersed-boundary method [*Peskin*, 1972; *Mittal and Iaccarino*, 2005] that inserts fictitious body forces into the equations of motion to mimic the presence of solid structures and internal boundaries. The resulting dynamics are such that velocity is negligible and pressure irrelevant within the solid matrix where the body forces are high. The particular technique employed is a variant of feedback forcing [*Goldstein et al.*, 1993], with implicit time discretization admitting rapid attenuation of the flow to stagnation within the solid matrix in $\mathcal{O}(\delta t)$ time comparable to the time step $\delta t = 5 \times 10^{-5}$ seconds of the fluid model. The flow simulations are run for 5×10^{-2} seconds with steady state conditions reached in $2 - 3 \times 10^{-2}$ seconds. The complete description of this methodology for resolving flow in explicit pore networks along with comparisons to other available methods are in [*SW10*], [*HSW12*], and *Siena et al.* [2012]. Nonetheless, the concept behind this method is provided for the reader's convenience.

Since we focus on gravity-driven flows of a homogeneous incompressible fluid (e.g. water) through a porous medium, the Navier-Stokes equations are,

$$
\begin{aligned}
\nabla \cdot \mathbf{v} &= 0, \qquad (6)\\
\frac{\partial \mathbf{v}}{\partial t} + \mathbf{v} \cdot \nabla \mathbf{v} &= -\nabla \pi' + \mathbf{g}' + \mu \triangle \mathbf{v} - \alpha \mathbf{v}.
\end{aligned}
$$

The primes refer to perturbations with respect to static ambient atmospheric conditions characterized by a constant density, ρ_0, and pressure, $p_0 = p_0(z)$, so $\pi' = (p - p_0)/\rho$ and $\mathbf{g}' = (0, 0, -g\rho'/\rho)$ where $\rho = \text{const} \gg \rho_0$ denotes the density of fluid and g is gravitational acceleration, g = 9.81 m/s^2. The kinematic viscosity of water, μ, is 10^{-6} ms^{-2}.

The last term on the right hand side of the momentum equation is the fictitious repelling body force of the immersed-boundary method, with a non-negative time scale $\alpha^{-1}(\mathbf{x}) = 0.5\delta t$ and the corresponding inverse time scale $\alpha(\mathbf{x}) = 0$ within the solid and fluid, respectively. Intuitively, setting $\alpha(\mathbf{x}) = 0$ within the fluid admits Navier-Stokes flows away from the solid boundaries, while requiring $\alpha(\mathbf{x}) \to \infty$ within the solid assures $\mathbf{v} \to 0$ there.

Unlike other immersed boundary methods, the pore space boundaries are aligned with grid nodes and the resulting media are simulated only with first-order accuracy in space. However, the macroscopic uncertainty of microscopic pore structure greatly exceeds numerical inaccuracies in the detailed representation of internal boundaries. Therefore, the first order approximation of a porous medium is adequate, at least for determining statistical bulk properties of the media and flow.

3.3. Variables for Transfer Functions

Porosity,

$$n = V_P/V, \tag{7}$$

is the ratio of void volume, V_p, over bulk volume, V, and measures the relative capacity of a porous medium to hold water. Mean hydraulic radius,

$$R = V_P/A_i, \tag{8}$$

is the ratio the void volume over the total interstitial area between the pore space and the solid matrix, A_i, and indicates the average level of connectivity in the network.

The tortuosity,

$$\tau(a,b) = l_S/l, \tag{9}$$

of a fluid particle trajectory connecting two points a and b is the ratio of the trajectory length, l_S, over the Euclidean distance between its end points, $l = ||a - b||$, hence $1 \leq \tau(a,b) < \infty$. A number of alternate definitions are in use including τ^2, τ^{-1}, and τ^{-2} [*Bear*, 1988]. The average tortuosity,

$$\bar{\tau} = \frac{1}{N}\sum_{i=1}^{N}\tau(a_i,b_i), \tag{10}$$

is taken over a sample of $i = 1, ..., N$ tortuosities, $\tau(a_i, b_i)$, each of which is derived from a particle trajectory that percolates through the entire medium. To determine the trajectory of a fluid particle, we follow [*HSW12*], and use every node in the void space at the top horizontal cross section as an initial position for a particle. To minimize the underestimation of tortuosity, only particles that percolate through the entire domain are included in the calculation of average tortuosity. The trajectory length, l_S, for every particle that percolates through the entire domain is used to compute tortuosity (9) and the average tortuosity for a pore space realization (10), cf., Section III. B of [*HSW12*] for a complete discussion.

[*HSW12*] and *Matyka et al.* [2008] both demonstrated that average tortuosity (10) is underestimated if the extent of the observation domain through which particles are tracked is not sufficiently large. Furthermore, as the extent of the observation domain increases the dependence on the extent of the domain decays exponentially, fluctuations in the computed values diminish, and a representative elementary volume with respect to tortuosity is observed for random virtual media.

Linear correlations among porosity, hydraulic radius, and tortuosity are significant across the entire data set (Table 2). The porosities of the glass beads and tuff are comparable to porosities for virtual media generated using the lowest value of the threshold parameter. Tortuosities and hydraulic radii of the beads and tuff are also comparable to those observed in the least permeable realizations of virtual media. The permeabilities and hydraulic radii of the data provided in *Mostaghimi et al.* [2013] are two to four orders of magnitude smaller than the stochastically generated pore networks used to derive the power laws, but have porosities comparable to the lower end of the synthetic media.

3.4. Permeability Estimates

Experimental estimates of permeability are obtained by applying Darcy's Law to the results of computational experiments with saturated pore spaces at steady state. By observing the pressure drop, Δp, and discharge of water, Q, from a column of sand of length L and cross-sectional area A, Darcy, [*Darcy*, 1856], established that discharge per unit area, Q/A, is proportional to the average pressure gradient, $\Delta p/L$, once steady-state is reached,

$$\frac{Q}{A} = -\frac{k}{\mu\rho}\frac{\Delta p}{L}. \tag{11}$$

The constant combines fluid density, ρ, and kinematic viscosity, μ, with permeability, k, a material characteristic of a porous medium; the ratio $K = k/(\mu\rho)$ is the saturated hydraulic conductivity of water according to Darcy.

Here, the permeability of each column of porous material bounded by solid walls on the lateral sides is estimated using the steady state velocity field, $\mathbf{v} = (u, v, w)$, and associated pressure field, p, of a fluid moving predominantly in the vertical direction. The total flux at a cross section of height z is estimated by

$$Q(z) = \int_A w(x, y, z)\chi(x, y, z)dxdy, \tag{12}$$

where χ is the characteristic (indicator) function within the porous material, $\chi(x, y, z) = 1$ in the void space and $\chi(x, y, z) = 0$ in the solid matrix. The total pressure is converted to hydraulic head, $h = (p - p_o)/(\rho g) + z - z_o$, where p_o is a reference pressure at the datum z_o and g is gravitational acceleration, and then the average hydraulic head at each cross section is estimated as

$$H(z) = \frac{1}{n(z)A}\int_A h(x, y, z)\chi(x, y, z)dxdy, \tag{13}$$

where $n(z)$ is the porosity of the cross section at the level z. Expressing (11) in terms of (12) and (13) and rearranging terms, the permeability at each cross section is estimated

$$k(z) = -\frac{\mu}{g}\frac{\int_A w(x, y, z)\chi(x, y, z)dxdy}{\Delta\{[n(z)]^{-1}\int_A h(x, y, z)\chi(x, y, z)dxdy\}/L}. \tag{14}$$

Because the dominant direction of flow is perpendicular to the cross sections, the average equivalent permeability for the entire sample is the harmonic average of the cross section permeabilities

$$k_e = L_z \left(\int_{L_z} \frac{1}{k(\zeta)} d\zeta \right)^{-1} . \tag{15}$$

In practice, the support volume of this procedure is the horizontal cross section of each column with a vertical extent of three vertical grid levels. This volume is used to compute a second order accurate centered difference approximation of the hydraulic gradient in the vertical direction and the total flux (12) at each horizontal cross section.

3.5. Grid Resolution

In order to select a practical resolution for large numbers of flow simulations, a preliminary investigation is performed to determine how variations in grid resolution influence the observed Darcy flux, $q = Q/A$ (11), and estimated permeability, k_e (15). Because the generation procedure of virtual media depends on the grid, a physical sample with fixed resolution is used to assess the grid resolution effects. Using a sub-volume of the column of glass beads, whose physical characteristics are discussed in Section 3.1.2, the grid is refined and coarsened to four different levels. Linear interpolation is used to map the data set between varying grid resolutions. Table 3 displays grid dimensions, discretization step size, δx, mean Darcy flux,

$$\bar{q} \equiv \frac{1}{L_z} \int_{L_z} q(\zeta) d\zeta, \tag{16}$$

average relative deviation from mean Darcy flux, Dev q, estimated permeability, k_e, average relative deviation from estimated permeability, Dev k_e, average tortuosity (10), and the variance of tortuosities for all four resolutions. Dev q and Dev k_e are defined as

$$\text{Dev q} \equiv \overline{|\bar{q} - q(z)|/|\bar{q}|} \quad \text{and} \quad \text{Dev } k_e \equiv \overline{|k_e - k(z)|/|k_e|}, \tag{17}$$

respectively, where the over-bar on the right hand side denotes vertical average as in (16).

Since the flow system is at steady-state, conservation of mass dictates that Dev q should be zero. On the other hand, Dev k_e is not similarly constrained and finer resolutions should yield better estimates of variations in permeability. The mean Darcy flux and estimated permeability are about the same for all grid resolutions; whereas the values of Dev q are relatively low, showing that conservation of mass is approximately satisfied, and improves with grid resolution, approaching first order asymptotic convergence as pointed out in the last paragraph of Section 3.2. The decreasing differences in average tortuosity and the convergence of the variance of tortuosity at finer grid resolution also indicate that the local flow field is better resolved with the finer mesh.

We supplement our convergence study for the integral characteristics of the Darcy flows with a local convergence study for three randomly selected and substantially separated locations in the vertical. Table 4 displays grid discretization size and the $\mathcal{L}^2$ difference between the probability distribution functions (pdf) generated by each component in the velocity vector, (u, v, w), and the pdfs generated by velocity components at the finest resolution. For each of the velocity components at all three levels the relative error from the finest mesh resolution solution exhibits the aforementioned first order convergence. Moreover, the error between finest and second finest resolution is small. Therefore, we select the second most refined grid, $\delta x = 1.e^{-4}$m, for computational affordability.

4. Generalized Pedotransfer Functions

The data consist of triples (k_i, n_i, R_i) for each of the $i = 1, \ldots, 63$ virtual pore spaces. Models, whose parameters are fitted through least squares, produce an estimate, $\hat{k}_i = \hat{k}(\eta_i)$, of permeability with η referring to n, R^2, or nR^2. To evaluate the performance of the models the independent real media data are withheld from the fitting and used to evaluate the goodness-of-fit through plots and overall chi-squared tests.

4.1. Empirical Pedotransfer Functions

When the data are fitted to the Kozeny equation (1), the Kozeny coefficient is $c_0 = 0.19$, which is essentially the same as Carman's original value of 1/5 [*Carman*, 1939] and falls within the range $[1/6, 1/2]$ that he gave later [*Carman*, 1956]. However, the relationship between permeability and the Kozney predictor is nonlinear over the ranges of sample data (Fig. 3). The Kozeny equation captures the basic rising trend of permeability with the Kozeny predictor, nR^2, but the requirement that the model goes through the origin, which is a necessary condition for a physically consistent law, constrains the performance of the Kozeny equation. The best fit linear model to these data, which is not shown, has a linear correlation of 0.9, but it does not go through the origin. The nominal 95% confidence intervals for the Kozeny equation are so wide that they easily include the independent real data. Confidence intervals are nominal in the sense that classic statistical formulae are used to calculate them, but the data do not meet independence and distributional criteria for statistical hypothesis testing. Nonetheless, the confidence intervals are useful for comparisons. For these purposes, a useful confidence interval is narrow, yet includes nearly all the data.

A better fit to the data can be attained using nonlinear models based on porosity n, hydraulic radius R^2, and their product nR^2. Three power law models to predict permeability, $\hat{k}(\eta) = a(\eta)^b$, are derived and compared to the linear Kozeny equation. The free parameters a and b are fitted using the nonlinear fit module in MATHEMATICA [*Wolfram*, 1999]. Due to the high correlation of tortuosity τ with n and R^2, τ is not used as a predictor variable in the power laws. All three power laws capture the nonlinear trend of the data and their confidence intervals are fairly tight including the independent real data (Fig. 4-6).

The sum of squared departures of the simulated data, $\hat{k}$, from the model estimates,

$$s_d^2 = \sum_{i=1}^{N_s} (\hat{k}_i - k_i)^2, \tag{18}$$

is the total variability in the data that is not accounted for by the models where N_s is the number of samples ($N_s = 63$ for this data set). The sum of squared departures of the Kozeny equation is an order of magnitude greater than those of the power laws (Table 5).

The additional parameter is one reason the power laws perform better than the Kozeny equation. A statistical method, the Analysis of Variance [*Mood et al.*, 1963], takes this into account by weighting the sum of squared departures with P, the number of parameters in the model, and comparing it to the model sum of squares,

$$s_M^2 = \sum_{i=1}^{N_s} (\hat{k}_i - \langle k \rangle)^2, \tag{19}$$

weighted by $N_s - P$, the degrees of freedom remaining in the sample after accounting for the parameters. The model sum of squares reflects the ability of the model to capture the structure of the data as departures from the sample mean, $\langle k \rangle$. The ratio,

$$F = \frac{s_M^2/P}{s_d^2/(N_s - P)}, \tag{20}$$

can be used to compare models: the larger is F, the better is the fit of the model. The F ratios of the predictor power law is about four times greater than that of the Kozeny equation despite the additional parameter (Table 6). The F ratios for the power laws based solely on n or R^2 are triple and double that of the Kozeny equation.

4.2. Range of Applicability

Porous media may fall into three classes. The first class consists of ordinary porous media with porosities in the approximate range $0.2 < n < 0.7$. In these cases, porosity is primary in the sense that it arises from voids in the material of the medium. In the second class there are barely permeable media with low porosities, $n < 0.2$. Often such media are composed of nearly solid rock with secondary channels arising from external mechanical or thermal stresses [*Davis*, 1988]. In these cases flow often corresponds to flow through a collection of discrete, sparsely connected pipes. Finally, the third class consists of highly permeable media where flow is similar to slow flows with obstructions that are relatively widely spaced, for instance fluidized beds. The porous media investigated here fall into either the first or third class.

When restricted to media of the first class, porosities $0.2 < n < 0.7$, a version of the Kozeny equation

$$k = 0.35nR^2, \tag{21}$$

provides reasonable estimates of permeability in agreement with the conclusions of *Xu and Yu* [2008]. In this range, the model (21) also provides a close fit to the real data (Fig. 7). Moreover, the computed Kozeny coefficient, $c_0 = 0.35$, is within the range $1/6 < c_0 < 1/2$ given by *Carman* [1956]. Within this normal range of porosity, the Kozeny-Carman equation (2) is

$$k = 0.45nR^2/\tau^2. \tag{22}$$

Carman [1956] mentions $c_0' = 0.40$ is plausible for non-circular sections.

The F ratio (20) for model (21) is $F = 1770.55$, which is greater than the F ratio obtained for the power laws based upon n or R^2 and thrice as large as that for the Kozeny equation fitted to the entire data set. However, the F ratio of model (22), $F = 551.09$, is less than half of that of (21).

The Kozeny equation does not account for variability over the full range of data as well as the power laws, having a sum of squared errors that is an order of magnitude greater than the power law models (Table 5). This is true even when the model sums of squares are adjusted for the number of parameters (Table 6).

Of the four models considered here, the power law based on the Kozeny predictor,

$$\hat{k} = 1.68 \cdot 10^{-4} (nR^2)^{0.58}, \tag{23}$$

fits the entire virtual data set best having an F ratio of 1866.17, which is nearly four times that of the Kozeny equation over the entire set and roughly double that of (21). Power laws based on porosity and hydraulic radius, the components of the Kozeny predictor, also give good fits to all the data. The exponent appears to account for nonlinear effects at the extremes of pore space interconnectivity consistent with observations of Jacquin [1964] quoted in [*Adler et al.*, 1990], *Lemaitre and Adler* [1990] and *Revil and Cathles* [1999].

Figures (3-6) indicate that the power-law models and the Kozeny equation fit the independent observed data well. However, the power-law based on porosity alone does not fit the low permeability samples obtained from *Mostaghimi et al.* [2013] as well as the other models. Nonetheless, the power laws are clearly superior to the Kozeny equation when the goodness of model fits is evaluated by chi-squared tests applied to both observed and virtual data (Table 7). Chi-squared tests are based on distances between model estimates and data weighted by the estimates [*Mood et al.*, 1963], and are used here qualitatively in the same spirit as the Analysis of Variance results reported earlier (Table 6). Small values of the chi-squared statistic indicate good fits, and the chi-squared values for the power laws are about five-six times smaller than the corresponding value for the Kozeny equation.

5. Summary and Conclusions

Kozeny derived his equation by equating the velocity given by Poiseuille's law for flow through an idealized pore network to the specific discharge obtained via Darcy's law; he determined that the permeability of a porous medium, k, is linearly proportional to the product nR^2 of its porosity, n, with the square of its mean hydraulic radius, R. This simplified model of a porous medium allowed him to attain an analytical solution to the governing equations of flow through porous media. However, topological alterations that make a pore network more realistic render analytical solutions nearly intractable. When applied over a wide range of porous media, computational experiments reveal a nonlinear relationship between permeability and its predictors, contrary to Kozeny's result. This nonlinearity is manifested by the wide range of values of the Kozeny coefficient observed at the extreme ends of porosity [*Sullivan*, 1942; *Kyan et al.*, 1970; *Davies and Dollimore*, 1980; *Adler et al.*, 1990; *Xu and Yu*, 2008]. On one hand, Kozeny's linear (in the predictor nR^2) approximation appears satisfactory within a restricted range of porosities, $0.2 < n < 0.7$. On the other hand, the nonlinearity cannot be adequately represented by a linear approximation when a wider range of porosity is considered.

We empirically derive three nonlinear generalized pedotransfer functions for permeability using computational experiments with flow through a set of stochastically generated pore networks with porosities ranging from 0.19 to 0.84 and varying degrees of connectivity. The transfer functions are power laws based on porosity n, mean hydraulic radius squared R^2, and their product nR^2; the same predictor which Kozeny used. The experimental pore networks consist of sixty-three virtual networks whose permeabilities, porosities, and mean hydraulic radii are used to estimate the parameters of the transfer functions. Porosity and mean hydraulic radius are observed directly from images of the pore networks and Darcy's law is used to compute the permeability from steady-state flow fields within the porous media.

When fitting the Kozeny equation to the full range of data, the computed value of the Kozeny coefficient computed is $c_0 = 0.19$, essentially the value originally suggested by Carman, $c_0 = 1/5$ [*Carman*, 1939]. However, the Kozeny equation does not provide good estimates of permeability over the full range of data, because of the nonlinear dependence of k on the Kozeny predictor, nR^2. On the other hand, the Kozeny equation is reasonably accurate within a limited range of of porosities (Fig. 7), but not for the originally suggested value of the Kozeny coefficient. Nonetheless, the estimated value of $c_0 = 0.35$ is within the wider range $1/6 < c_0 < 1/2$ that Carman gave later [*Carman*, 1956].

All of the transfer functions include the fifteen independent real data samples within nominal 95% confidence intervals. The power laws fit the data in this study better than the Kozeny equation, even when they are penalized through an Analysis of Variance for including an additional model parameter (Table 5-6). The leading coefficient of each power law is an empirical fitting parameter and has dimensions of $L^{2(1-b)}$, where b is the power appearing in Table 5. Only in specialized cases, such as the Kozeny equation are the associated coefficients dimensionless. Similar functions to predict permeability having coefficients with dimensions are already present in the literature [*Katz and Thompson*, 1986; *Ahuja et al.*, 1989; *Rodriguez et al.*, 2004; *Costa*, 2006].

The equation

$$\hat{k} = 1.68 \cdot 10^{-4}(nR^2)^{0.58} \tag{24}$$

provides the best fit to the full range of data. Additionally, its confidence intervals are tighter, its sum of squared departures is smaller, and its F (20) ratio is higher than any of the other models considered.

Even though Kozeny derived his equation through microscopic considerations, it has been applied on macroscopic scales as a generalized pedotransfer function. Commonly, pedotransfer functions are derived empirically using various soil samples in continuum scale laboratory experiments where the predictors, e.g., porosity and mean hydraulic radius, can be measured in bulk.

The virtual networks that are the basis for these transfer functions are homogeneous and isotropic with porosities and mean hydraulic radii spanning a wide range of representative values. Sample permeabilities are comparable to those found in well- sorted sands or sands and gravel. Since the networks are large enough to constitute representative elementary volumes [*HSW12*], the physical basis and scale of these experiments is comparable to that which Kozeny used. Moreover, the derived pedotransfer functions are not formally limited to representations of explicit pore spaces or a particular soil type because porosity and hydraulic radius can be estimated in bulk using field observations or laboratory experiments and are general traits of porous media. As a result, it should be possible to test whether the proposed generalized pedotransfer functions apply in the field.

Acknowledgments. We wish to thank Dorthe Wildenschild of Oregon State University for generously sharing her tuff and bead data sets with us. We also thank an anonymous referee for bringing the recently published data of *Mostaghimi et al.* [2013] to our attention. We also want to thank Alberto Guadagnini, Monica Riva, and Martina Siena for commenting on early drafts of this paper and Shlomo Neuman for several discussions. J.D.H. acknowledges the support of the Graduate Visitor Program, a part of the Advanced Study Program at the National Center for Atmospheric Research. P.K.S acknowledges partial support by the DOE awards #DE-FG02-08ER64535 and #DE-SC0006748, and the NSF grant OCI-0904599 while conducting this work. The National Center for Atmospheric Research is sponsored by the National Science Foundation.

References

Abiodun, B. J., W. J. Gutowski, and J. M. Prusa, Implementation of a non-hydrostatic, adaptive-grid dynamics core in CAM3. part ii: dynamical influences on itcz behavior and tropical precipitation, *Climate Dynam.*, *31*(7), 811–822, 2008a.

Abiodun, B. J., J. M. Prusa, and W. J. Gutowski, Implementation of a non-hydrostatic, adaptive-grid dynamics core in CAM3. part i: comparison of dynamics cores in aqua-planet simulations, *Climate Dynam.*, *31*(7), 795–810, 2008b.

Adler, P. M., and C. G. Jacquin, Fractal porous media i: Longitudinal stokes flow in random carpets, *Trans. Porous Med.*, *2*(6), 553–569, 1987.

Adler, P. M., C. G. Jacquin, and J. A. Quiblier, Flow in simulated porous media, *Int. J. Multiphas Flow*, *16*(4), 691–712, 1990.

Ahuja, L. R., D. K. Cassel, R. R. Bruce, and B. B. Barnes, Evaluation of spatial distribution of hydraulic conductivity using effective porosity data, *Soil Sci.*, *148*(6), 404, 1989.

Alexander, K. S., Percolation and minimal spanning forests in infinite graphs, *Ann. Probab.*, pp. 87–104, 1995.

Alexander, K. S., and S. A. Molchanov, Percolation of level sets for two-dimensional random fields with lattice symmetry, *J. Stat. Phys.*, *77*(3), 627–643, 1994.

Archie, G. E., The electrical resistivity log as an aid in determining some reservoir characteristics, *Trans. AIMe*, *146*(99), 54–62, 1942.

Bear, J., *Dynamics of fluids in porous media*, Dover publications, 1988.

Carman, P. C., Permeability of saturated sands, soils and clays, *J. Agric. Sci*, *29*, 262–273, 1939.

Carman, P. C., *Flow of gases through porous media*, Butterworths Scientific Publications London, 1956.

Chapuis, R. P., and M. Aubertin, On the use of the Kozeny-Carman equation to predict the hydraulic conductivity of soils, *Can. Geotech. J.*, *40*(3), 616–628, 2003.

Costa, A., Permeability-porosity relationship: A reexamination of the Kozeny-Carman equation based on a fractal pore-space geometry assumption, *Geophys. Res. Lett.*, *33*(2), L02,318, 2006.

Culligan, K. A., D. Wildenschild, B. S. B. Christensen, W. G. Gray, M. L. Rivers, and A. F. B. Tompson, Interfacial area measurements for unsaturated flow through a porous medium, *Water Resour. Res.*, *40*(12), W12,413, 2004.

Darcy, H. P. G., Les fontaines publiques de la ville de Dijon, Victor Dalmont, Paris. cf. Muskat, M, *The Flow of Homogeneous Fluids Through Porous Media*, 1856.

Davies, L., and D. Dollimore, Theoretical and experimental values for the parameter K of the Kozeny-Carman equation, as applied to sedimenting suspensions, *J. Phys. D: Appl. Phys.*, *13*, 2013, 1980.

Davis, S. N., Sandstones and shales, *Hydrogeology: Boulder, Colorado, Geological Society of America, The geology of North America*, *2*, 323–332, 1988.

Dvorkin, J., Kozeny-Carman equation revisited, 2009.

Fourie, W., R. Said, P. Young, and D. L. Barnes, The simulation of pore scale fluid flow with real world geometries obtained from X-ray computed tomography, in *Proceedings of the Boston COMSOL Conference*, 2007.

Ghizaru, M., P. Charbonneau, and P. K. Smolarkiewicz, Magnetic cycles in global large-eddy simulations of solar convection, *Astrophys J. Lett.*, *715*, L133, 2010.

Goldstein, D., R. Handler, and L. Sirovich, Modeling a no-slip flow boundary with an external force field, *J. Comput. Phys.*, *105*(2), 354–366, 1993.

Grabowski, W. W., and P. K. Smolarkiewicz, A multiscale anelastic model for meteorological research, *Monthly Weather Rev.*, *130*(4), 939–956, 2002.

Hasimoto, H., On the periodic fundamental solutions of the Stokes equations and their application to viscous flow past a cubic array of spheres, *J. Fluid Mech*, *5*(02), 317–328, 1959.

Heijs, A. W. J., and C. P. Lowe, Numerical evaluation of the permeability and the Kozeny constant for two types of porous media, *Phys. Rev. E*, *51*(5), 4346, 1995.

Hyman, J. D., P. K. Smolarkiewicz, and C. L. Winter, Heterogeneities of flow in stochastically generated porous media, *Phys. Rev. E*, *86*, 056,701, doi: 10.1103/PhysRevE.86.056701, 2012.

Katz, A. J., and A. H. Thompson, Quantitative prediction of permeability in porous rock, *Phys. Rev. B*, *34*(11), 8179–8181, 1986.

Koponen, A., M. Kataja, and J. Timonen, Tortuous flow in porous media, *Phys. Rev. E*, *54*(1), 406, 1996.

Koponen, A., M. Kataja, and J. Timonen, Permeability and effective porosity of porous media, *Phys. Rev. E*, *56*(3), 3319, 1997.

Kozeny, J., *SB Akad. Wiss. Wien*, *136a*, 271, 1932.

Kyan, C. P., D. T. Wasan, and R. C. Kintner, Flow of single-phase fluids through fibrous beds, *Ind. Eng. Chem. Fund.*, *9*(4), 596–603, 1970.

Launder, B. E., and T. H. Massey, The numerical prediction of viscous flow and heat transfer in tube banks, *J. Heat Transf.*, *100*, 565, 1978.

Lebron, I., M. G. Schaap, and D. L. Suarez, Saturated hydraulic conductivity prediction from microscopic pore geometry measurements and neural network analysis, *Water Resour. Res.*, *35*(10), 3149–3158, 1999.

Lemaitre, R., and P. M. Adler, Fractal porous media iv: Three-dimensional stokes flow through random media and regular fractals, *Trans. Porous Med.*, *5*(4), 325–340, 1990.

Matyka, M., A. Khalili, and Z. Koza, Tortuosity-porosity relation in porous media flow, *Phys. Rev. E*, *78*(2), 026,306, 2008.

Meakin, P., and A. M. Tartakovsky, Modeling and simulation of pore-scale multiphase fluid flow and reactive transport in fractured and porous media, *Rev. Geophys.*, *47*(3), RG3002, 2009.

Mittal, R., and G. Iaccarino, Immersed boundary methods, *Annu. Rev. Fluid Mech.*, *37*, 239–261, 2005.

Mood, A. M., F. A. Graybill, and D. C. Boes, *Introduction into the theory of statistics*, McGraw-Hill International Book Company, 1963.

Mostaghimi, P., M. Blunt, and B. Bijeljic, Computations of absolute permeability on micro-CT images, *Math Geosci.*, *45*, 103–125, 2013.

Nabovati, A., E. W. Llewellin, and A. Sousa, A general model for the permeability of fibrous porous media based on fluid flow simulations using the lattice Boltzmann method, *Compos. Part A - Appl. S.*, *40*(6), 860–869, 2009.

Nielsen, D. R., L. R. Ahuja, and J. W. Naney, Scaling soil water properties and infiltration modeling, *Soil Sci. Soc. Am. J.*, *48*(5), 970–973, 1984.

Ortiz, P., and P. K. Smolarkiewicz, Coupling the dynamics of boundary layers and evolutionary dunes, *Phys. Rev. E*, *79*(4), 041,307, 2009.

Peskin, C. S., Flow patterns around heart valves: a numerical method, *J. Comput. Phys.*, *10*(2), 252–271, 1972.

Prusa, J. M., P. K. Smolarkiewicz, and A. A. Wyszogrodzki, EULAG, a computational model for multiscale flows, *Comput. Fluids*, *37*(9), 1193–1207, 2008.

Rawls, W. J., A. Nemes, and Y. A. Pachepsky, Influence of organic matter on the estimation of saturated hydraulic conductivity, *Soil Sci. Soc. Am. J.*, *69*(4), 1330–1337, 2005.

Revil, A., and L. M. Cathles, Permeability of shaly sands, *Water Resour. Res.*, *35*(3), 651–662, 1999.

Rodriguez, E., F. Giacomelli, and A. Vazquez, Permeability-porosity relationship in rtm for different fiberglass and natural reinforcements, *J. Compos. Mat.*, *38*(3), 259–268, 2004.

Rubinstein, J., Effective equations for flow in random porous media with a large number of scales, *J. Fluid Mech.*, *170*(1), 379–383, 1986.

Sangani, A., and A. Acrivos, Slow flow through a periodic array of spheres, *Int. J. Multiphas. Flow*, *8*(4), 343–360, 1982a.

Sangani, A. S., and A. Acrivos, Slow flow past periodic arrays of cylinders with application to heat transfer, *Int. J. Multiphas. Flow*, *8*(3), 193–206, 1982b.

Schaap, M. G., and I. Lebron, Using microscope observations of thin sections to estimate soil permeability with the Kozeny-Carman equation, *J. Hydrol.*, *251*(3-4), 186–201, 2001.

Schaap, M. G., F. J. Leij, and M. T. van Genuchten, Rosetta: A computer program for estimating soil hydraulic parameters with hierarchical pedotransfer functions, *J. Hydrol.*, *251*(3), 163–176, 2001.

Sen, P. N., C. Scala, and M. H. Cohen, A self-similar model for sedimentary rocks with application to the dielectric constant of fused glass beads, *Geophysics*, *46*(5), 781–795, 1981.

Shvidler, M. I., *Filtration flows in heterogeneous media: a statistical approach*, Consultants Bureau, 1964.

Siena, M., A. Guadagnini, M. Riva, P. Gouze, P.K. Smolarkiewicz, C.L. Winter, J.D. Hyman, F. Inzoli, G. Gudon, and E. Colombo, A comparison of body-fitted and immersed boundary methods for pore- scale modeling of fully saturated flow in synthetic porous media, in *Proceedings of the 2012 IAHR International Groundwater Symposium, Kuwait, 1-8, 2012.*, 2012.

Smolarkiewicz, P. K., and C. L. Winter, Pores resolving simulation of Darcy flows, *J. Comput. Phys.*, *229*(9), 3121–3133, 2010.

Smolarkiewicz, P. K., R. Sharman, J. Weil, S. G. Perry, D. Heist, and G. Bowker, Building resolving large-eddy simulations and comparison with wind tunnel experiments, *J. Comput. Phys.*, *227*(1), 633–653, 2007.

Sullivan, R. R., Specific surface measurements on compact bundles of parallel fibers, *J. Appl. Phys.*, *13*(11), 725–730, 1942.

Waite, M. L., and P. K. Smolarkiewicz, Instability and breakdown of a vertical vortex pair in a strongly stratified fluid, *J. Fluid Mech.*, *606*(1), 239–273, 2008.

Wedi, N. P., and P. K. Smolarkiewicz, Direct numerical simulation of the plumb-mcewan laboratory analog of the QBO, *J. Atmo. Sci.*, *63*(12), 3226–3252, 2006.

Whitaker, S., *The method of volume averaging*, vol. 13, Springer Netherlands, 1999.

Wildenschild, D., K. A. Culligan, and B. S. B. Christensen, Application of X-ray microtomography to environmental fluid flow problems. in developments in X-ray tomography, *Proceedings of SPIE*, *5535*, 432–441, 2004.

Wolfram, S., *The mathematica book*, Cambridge university press, 1999.

Wösten, J. H. M., Y. A. Pachepsky, and W. J. Rawls, Pedotransfer functions: bridging the gap between available basic soil data and missing soil hydraulic characteristics, *J. Hydrol.*, *251*(3), 123–150, 2001.

Xu, P., and B. Yu, Developing a new form of permeability and Kozeny-Carman constant for homogeneous porous media by means of fractal geometry, *Adv. Water Resour.*, *31*(1), 74–81, 2008.

Zick, A., and G. M. Homsy, Stokes flow through periodic arrays of spheres, *J. Fluid Mech.*, *115*, 13–26, 1982.

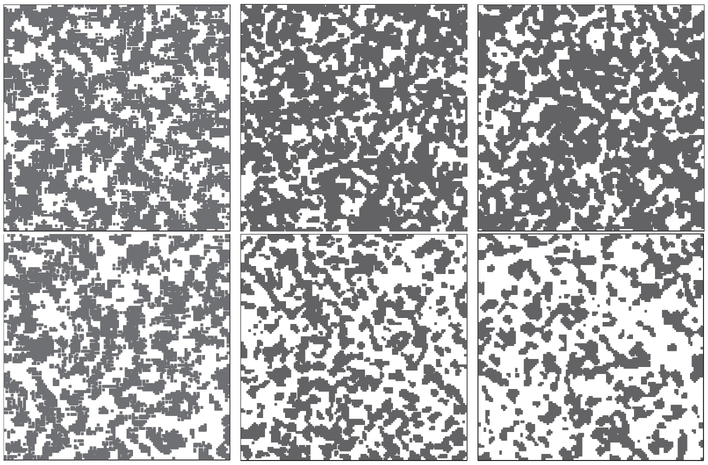

Figure 1. Porespace cross-sections in the x-y plane (1.27 cm $\times$ 1.27 cm). From left to right : uniform kernel, Gaussian kernel, and iterative method; top, Threshold Parameter 0.45 (Expected Porosity $\approx$ 0.35) ; bottom, Threshold Parameter 0.53 (Expected Porosity $\approx$ 0.60).

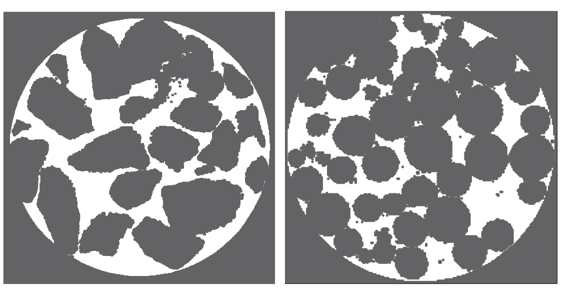

Figure 2. Physical porous media: tuff (left) and glass beads (right); corresponding values of (n, τ, R) are (0.37, 1.23, 9.12$\cdot10^{-5}$ m) and (0.31, 1.20, 2.89$\cdot10^{-5}$ m.)

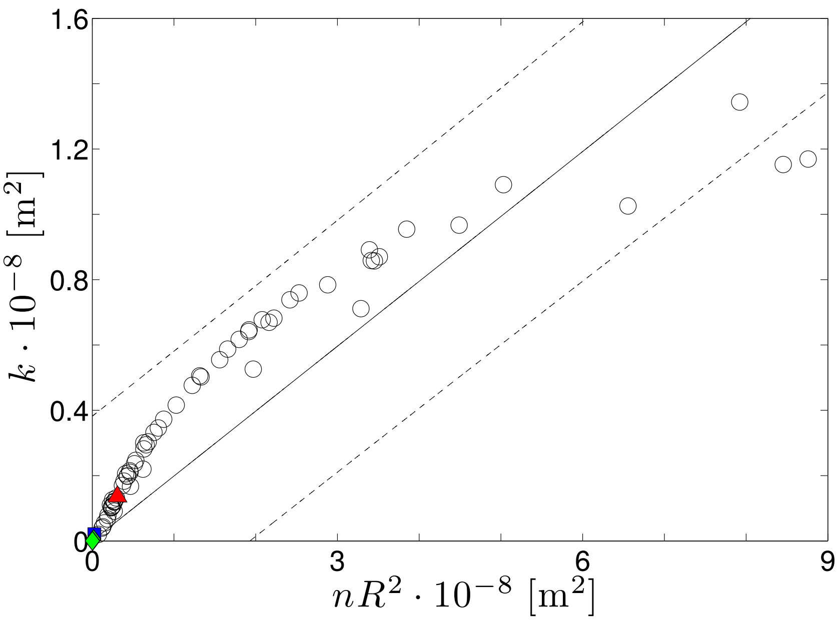

Figure 3. Kozeny equation $k(nR^2) = c_0 nR^2$. Points correspond to averaged amounts for each of the 63 stochastic realizations and fifteen sets of natural data. Circles, blue square, red triangle, and green diamonds denote synthetic data, glass beads, tuff, and the low permeability data of *Mostaghimi et al.* [2013] respectively. Least-squares models are solid lines, and nominal 95% confidence intervals are dashed lines.

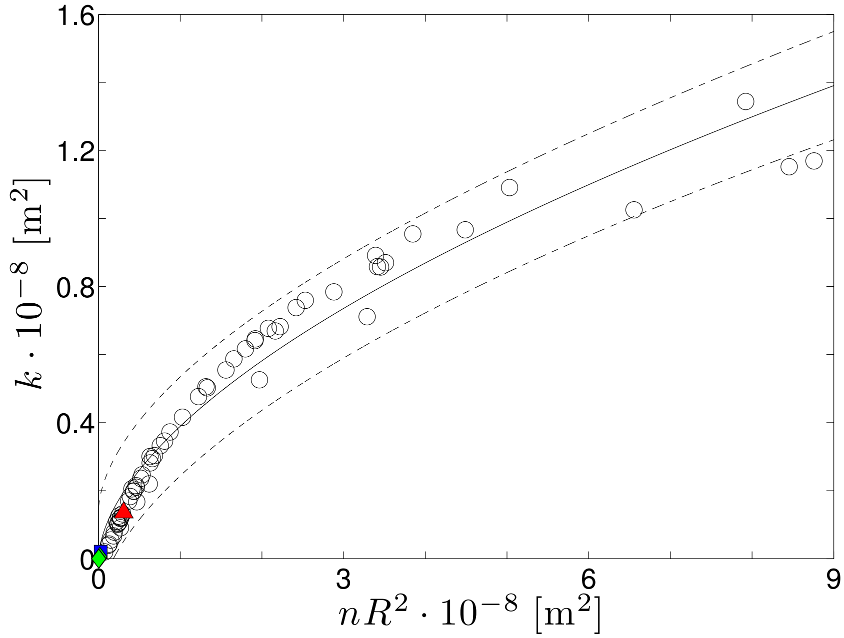

Figure 4. As in Fig. 3 but for power law $k(R^2) = a(R^2)^b$.

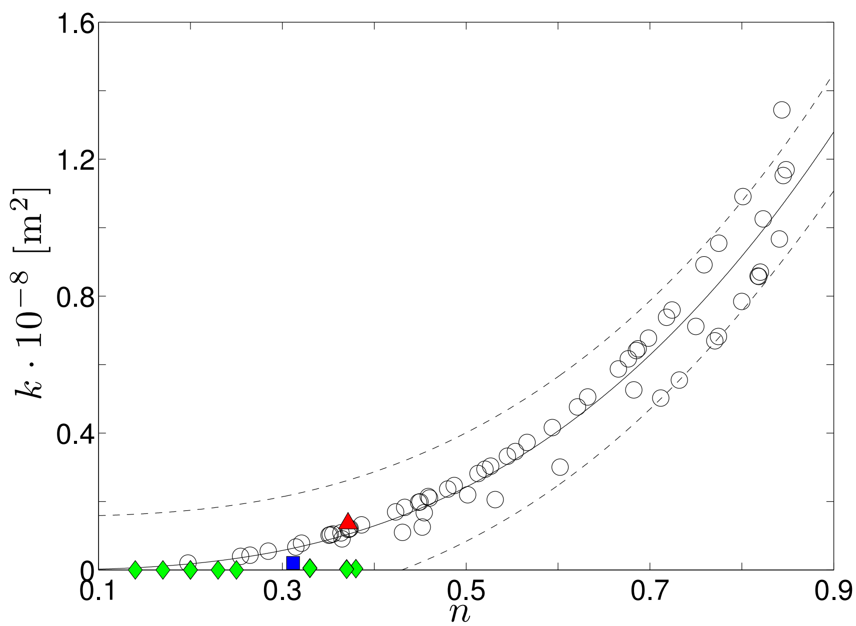

Figure 5. As in Fig. 3 but for power law $k(n) = an^b$.

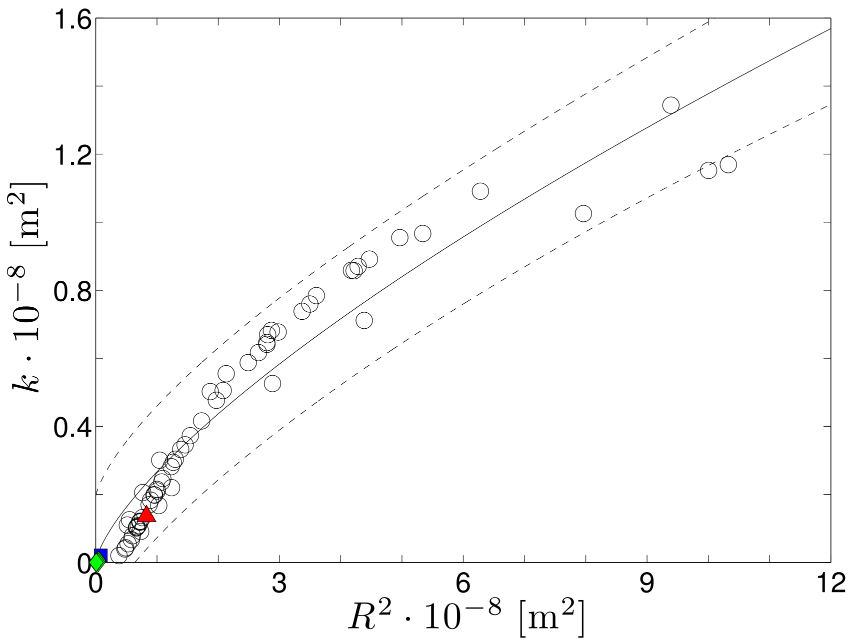

Figure 6. As in Fig. 3 but for power law $k(n) = a(nR^2)^b$.

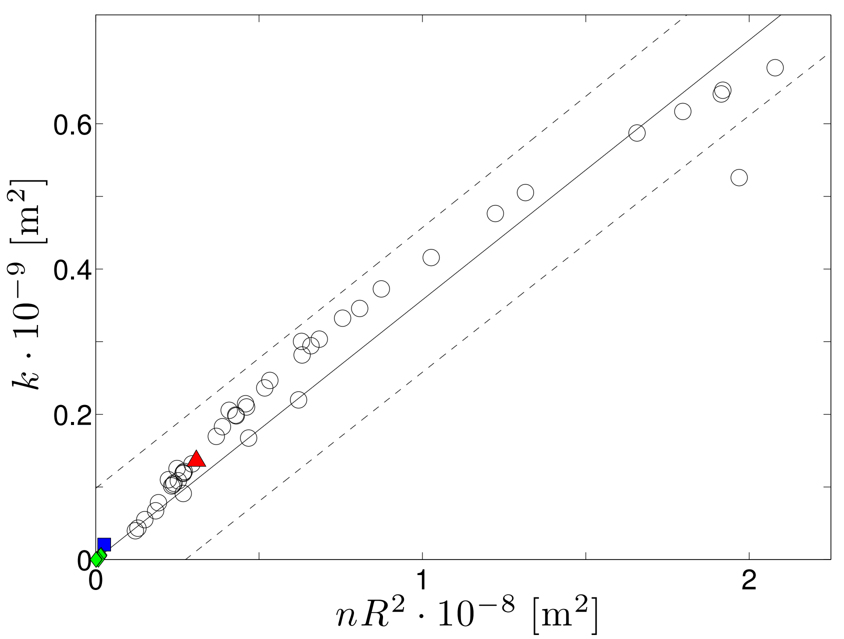

Figure 7. Kozeny equation fitted to porous media with normal porosities, $0.2 < n < 0.7$; Circles, square, triangle, and diamonds denote synthetic data, glass beads, tuff, and the low permeability data of *Mostaghimi et al.* [2013] respectively.

Table 1. Characteristics of virtual media in Fig. 1.

	Uniform	Gaussian	Iterative
$\gamma = 0.45$ (Expected Porosity ≈ 0.35) :			
k [a]	$1.10 \cdot 10^{-9}$	$1.32 \cdot 10^{-9}$	$9.10 \cdot 10^{-10}$
n [b]	0.43	0.38	0.36
R^2 [c]	$5.16 \cdot 10^{-9}$	$7.63 \cdot 10^{-9}$	$7.33 \cdot 10^{-9}$
nR^2 [d]	$2.22 \cdot 10^{-9}$	$2.94 \cdot 10^{-9}$	$2.68 \cdot 10^{-9}$
τ [e]	1.25	1.23	1.33
$\gamma = 0.53$ (Expected Porosity ≈ 0.60) :			
k [a]	$3.00 \cdot 10^{-9}$	$4.76 \cdot 10^{-9}$	$5.26 \cdot 10^{-9}$
n [b]	0.60	0.62	0.68
R^2 [c]	$1.05 \cdot 10^{-8}$	$1.97 \cdot 10^{-8}$	$2.88 \cdot 10^{-8}$
nR^2 [d]	$6.30 \cdot 10^{-9}$	$1.22 \cdot 10^{-8}$	$1.97 \cdot 10^{-8}$
τ [e]	1.16	1.12	1.14

[a] Permeability [m^2]

[b] Porosity

[c] Hydraulic radius squared [m^2]

[d] Kozeny predictor [m^2]

[e] Tortuosity

Table 2. Correlations among predictor variables.

	n	R	τ
n	1.00	0.90	-0.95
R	0.90	1.00	-0.84
τ	-0.95	-0.84	1.00

Table 3. Grid Resolution Study

n × m × l [a]	δx [b]	$\bar{q}$ [c]	Dev q [%] [d]	k_e [e]	Dev k$_e$ [%] [f]	$\bar{\tau}$ [g]	$\sigma(\tau)$ [h]
$18 \times 18 \times 38$	4.e-04	-2.00e-02	1.16	2.04e-09	121.86	1.25	1.54e-02
$36 \times 36 \times 76$	2.e-04	-2.08e-02	0.86	2.12e-09	117.08	1.28	2.11e-02
$72 \times 72 \times 150$	1.e-04	-2.12e-02	0.39	2.16e-09	202.41	1.31	2.21e-02
$144 \times 144 \times 300$	5.e-05	-2.02e-02	0.22	2.06e-09	215.61	1.31	2.22e-02

[a] Grid dimensions

[b] Grid discretization [m]

[c] Mean Darcy flux [m/s]

[d] Average relative deviation from the mean Darcy flux [%]

[e] Estimated permeability [m^2]

[f] Average relative deviation from estimated permeability [%]

[g] Average Tortuosity

[h] Variance of Tortuosities

Table 4. Local Grid Resolution Study

	Level 1			Level 2			Level 3		
δx [a]	$L^2(u)$ [b]	$L^2(v)$ [c]	$L^2(w)$ [d]	$L^2(u)$ [b]	$L^2(v)$ [c]	$L^2(w)$ [d]	$L^2(u)$ [b]	$L^2(v)$ [c]	$L^2(w)$ [d]
4.e-04	1.73e-01	1.44e-01	1.15e-01	1.48e-01	1.14e-01	1.19e-01	1.46e-01	1.22e-01	1.04e-01
2.e-04	7.33e-02	7.01e-02	5.65e-02	6.41e-02	5.25e-02	5.20e-02	7.36e-02	6.93e-02	5.50e-02
1.e-04	3.39e-02	4.10e-02	3.25e-02	3.07e-02	2.75e-02	3.24e-02	3.20e-02	3.14e-02	2.98e-02

[a] Grid discretization [m]

[b] L^2 difference between pdf of u and pdf of u at finest resolution

[c] L^2 difference between pdf of v and pdf of v at finest resolution

[d] L^2 difference between pdf of w and pdf of w at finest resolution

Table 5. Accuracy of the four fitted models.

Model Form	Fit	s_d^2
$k(nR^2) = c_0 nR^2$	$\hat{k} = 0.19nR^2$	$2.26 \cdot 10^{-16}$
$k(nR^2) = a(nR^2)^b$	$\hat{k} = 1.68 \cdot 10^{-4}(nR^2)^{0.58}$	$3.15 \cdot 10^{-17}$
$k(n) = an^b$	$\hat{k} = 1.72 \cdot 10^{-8}(n)^{2.83}$	$3.72 \cdot 10^{-17}$
$k(R^2) = aR^{2b}$	$\hat{k} = 1.37 \cdot 10^{-3}(R^2)^{0.71}$	$5.61 \cdot 10^{-17}$

Table 6. Analysis of Variance

Model	P	s_M^2/P	$N_s - P$	$s_d^2/(N_s - P)$	F
Kozeny eq.	1	$1.74 \cdot 10^{-15}$	62	$3.65 \cdot 10^{-18}$	475.77
power law $k(nR^2)$	2	$9.65 \cdot 10^{-16}$	61	$5.16 \cdot 10^{-19}$	1866.17
power law $k(n)$	2	$9.62 \cdot 10^{-16}$	61	$6.11 \cdot 10^{-19}$	1574.55
power law $k(R^2)$	2	$9.52 \cdot 10^{-16}$	61	$9.20 \cdot 10^{-19}$	1034.89

Table 7. Chi Squared Statistics

Model	χ^2 Statistics
Kozeny eq.	$7.57 \cdot 10^{-08}$
power law $k(nR^2)$	$1.12 \cdot 10^{-08}$
power law $k(n)$	$1.19 \cdot 10^{-08}$
power law $k(R^2)$	$1.76 \cdot 10^{-08}$